Compressive axial mechanical properties of rat bone as functions of bone volume fraction, apparent density and micro-ct based mineral density

Esther Cory [a,1], Ara Nazarian [a,1], Vahid Entezari [a], Vartan Vartanians [a], Ralph Müller [c], Brian D. Snyder [a,b,*]

[a] *Center for Advanced Orthopedic Studies, Beth Israel Deaconess Medical Center and Harvard Medical School, Boston, MA, USA*
[b] *Department of Orthopedic Surgery, Children's Hospital, Harvard Medical School, Boston, MA, USA*
[c] *Institute of Biomechanics, Swiss Federal Institute of Technology, Zürich, Switzerland*

ARTICLE INFO

ABSTRACT

Mechanical testing has been regarded as the gold standard to investigate the effects of pathologies on the structure–function properties of the skeleton. With recent advances in computing power of personal computers, virtual alternatives to mechanical testing are gaining acceptance and use. We have previously introduced such a technique called structural rigidity analysis to assess mechanical strength of skeletal tissue with defects. The application of this technique is predicated upon the use of relationships defining the strength of bone as a function of its density for a given loading mode. We are to apply this technique in rat models to assess their compressive skeletal response subjected to a host of biological and pharmaceutical stimulations. Therefore, the aim of this study is to derive a relationship expressing axial compressive mechanical properties of rat cortical and cancellous bone as a function of equivalent bone mineral density, bone volume fraction or apparent density over a range of normal and pathologic bones.

We used bones from normal, ovariectomized and partially nephrectomized animals. All specimens underwent micro-computed tomographic imaging to assess bone morphometric and densitometric indices and uniaxial compression to failure.

We obtained univariate relationships describing 71–78% of the mechanical properties of rat cortical and cancellous bone based on equivalent mineral density, bone volume fraction or apparent density over a wide range of density and common skeletal pathologies. The relationships reported in this study can be used in the structural rigidity analysis introduced by the authors to provide a non-invasive method to assess the compressive strength of bones affected by pathology and/or treatment options.

© 2009 Elsevier Ltd. All rights reserved.

1. Introduction

Conventional mechanical testing has historically been regarded as the gold standard for investigating the effects of various interventions and pathologies on the structure–function properties of the skeleton (Danielsen et al., 1993; Turner and Burr, 1993; Hornby et al., 2003). Given the recent advances in speed, resolution, and reduction of artifacts in medical imaging (Genant et al., 2000; MacNeil and Boyd, 2007), and ever increasing computing power of personal computers (Moore, 1965), virtual alternatives to conventional invasive procedures are becoming increasingly feasible (Bagi et al., 1992; Ferretti et al., 1995; Ferretti et al., 1996; Van Rietbergen et al., 1999; Newitt et al.,

2002; van Rietbergen et al., 2002; Martin et al., 2004). Virtual Biomechanics, or the assessment of mechanical strength of skeletal tissue through alternate non-destructive means, enables one to perform longitudinal *in-vivo* assessment of bone strength to reduce the number of subjects and the costs associated with a study and facilitate the evaluation of multiple skeletal sites from the same subject. It can also reduce the large experimental errors associated with operator dependent procedures such as specimens prepration and gripping (Odgaard and Linde, 1991; Keaveny et al., 1997; Un et al., 2006) and inter-laboratory testing protocol differences (Turner, 1989).

Virtual alternatives to mechanical testing often account for the contribution of both tissue material and geometric properties to bone strength. Currently used methods of virtual biomechanics can be categorized into patient specific finite element analysis (FEA) (Martin, 1991; Bessho et al., 2007; Bonnick, 2007) and direct strength assessment based on Dual-energy X-ray Absorptiometry (DXA) (Leichter et al., 1982; Kanis et al., 2000) or quantitative computed tomography (QCT) (Gasser, 1995; Jamsa et al., 1998;

* Corresponding author at: Center for Advanced Orthopedic Studies, 330 Brookline Avenue, RN115, Boston, MA 02215, USA. Tel.: +1 617 667 2940; fax: +1 617 667 7175.

E-mail address: bsnyder@bidmc.harvard.edu (B.D. Snyder).
[1] These authors contributed equally to this work.

Lochmuller et al., 2002; Buckley et al., 2007). While patient specific FEA accounts for changes in tissue material and geometric properties, its main drawback is the cost associated with it, as this method requires large computational power and expert man-power to generate an appropriate model from medical imaging data (Guldberg et al., 1998). DXA is more cost-effective; but, fracture predictions based on DXA rely on a 2D projection of a 3D structure that do not take into account changes in either the material or geometric properties of bone and have been shown to be neither sensitive nor specific (Cummings et al., 2002; Riggs and Melton, 2002; Heaney, 2003; Bauer et al., 2004; Schuit et al., 2004). QCT based methods (Lang et al., 1988; Faulkner et al., 1991; Lang et al., 1997; Lang et al., 1998; Beck et al., 2000; Beck, 2003) are more accurate and provide information on both material and geometric properties of bone, yet they expose the patients to significant radiation dosages.

To that end, we have introduced a new method called Structural Rigidity Analysis (SRA) to supplement the currently available FE, QCT and DXA based methods to non-invasively assess the axial, bending and torsional rigidities of bones "with defect" from their transaxial cross-sectional images (Hong et al., 2004) in a series of *ex-vivo* (Whealan et al., 2000; Hong et al., 2004) and *in-vivo* (Aaron et al., 2002; Snyder et al., 2006) human experiments. With this technique, modulus of elasticity is treated as a function of bone density, and bone geometry is represented by its cross-sectional area and moment of inertia (Martin, 1991; Turner, 2002). For these studies, species-specific relationships for cancellous (Rice et al., 1988) and cortical (Snyder and Schneider, 1991) bone mechanical properties were used to express modulus of elasticity as a function of bone density. In order to extend the application of virtual biomechanics to animal models, validating empirical relationships that describe mechanical properties of any bone as a function of its density would be immensely beneficial.

Moreover, using separate models for the mechanical properties of cortical and cancellous bone, necessitates the introduction of an arbitrary thresholding value to separate cortical bone from cancellous bone. In order to void the use of such an arbitrary thresholding value; we will use nano-indentation (Ashman and Rho, 1988; Rho et al., 1998; Turner et al., 1999; Zysset et al., 1999) to demonstrate that tissue level modulus and hardness of rat cortical and cancellous bone are not different from one another, and that meaningful differences between the tissue types are best observed at the bone structural level. Therefore, a single univariate relationship between elastic modulus and density that spans both cortical and cancellous bone will be sought in the current study. This approach will facilitate further automation of the process; and reduce operator interventions which are prone to error.

To that end, we utilized micro-computed tomography (μCT) as the current research imaging tool of choice for non-destructive assessment of the three dimensional (3D) microstructural and densitometric properties of cancellous and cortical bone (Rueg-segger et al., 1996; Borah et al., 2001). The normal control (CON), ovariectomized (OVX) and partially nephrectomized (NFR) Spra-gue-Dawley (SD) rats were used as common animal models in bone research (An and Friedman, 1999) to represent a broad range of densities, and two predominant disease models that affect bone structure and material separately. *We hypothesize that at the macro level, either equivalent bone mineral density, bone volume fraction or apparent density account for the majority of changes in the mechanical properties of cortical and cancellous SD rat bone.* Therefore, we aim to derive univariate relationships expressing axial compressive mechanical properties of rat bone as a function of μCT based equivalent bone mineral density, bone volume fraction or apparent density over a range of normal and pathologic bones.

2. Methods

2.1. Animal model

The study protocol was approved by Beth Israel Deaconess Medical Center's Institutional Animal Care and Use Committee (IACUC). Thirty female Sprague-Dawley (SD, mass: 250–275 g, ~15 weeks old) rats were obtained from Charles River Laboratories (Charles River, Charlestown, MA, USA) and were divided into three equally sized groups: the animals in the control group were not subjected to any surgical or dietary interventions; the OVX group underwent ovariectomy (a week prior to the start of the study) to induce a state of low bone mass and micro-architectural deterioration (Miller and Wronski, 1993; Guo and Goldstein, 2000; Wang et al., 2001; Hornby et al., 2003; Ito et al., 2005; Kaczmarczyk-Sedlak et al., 2005; Ogawa et al., 2005; Reddy Nagareddy and Lakshmana, 2005; Yao et al., 2005); and the NFR group underwent $\frac{5}{6}$ nephrectomy (Freesmeyer et al., 2001; Jokihaara et al., 2006) (a week prior to the start of the study) in addition to being placed on a modified diet containing 0.6% Ca and 1.2% P (from time zero till the end of the study) to induce renal osteodystrophy (normal rodent diet contains 1.35% Ca and 1.04% P) and severe secondary hyperparathyroidism (Turner et al., 1996; Miller et al., 1998; Freesmeyer et al., 2001; Kazama et al., 2003; Brkovic et al., 2005; Feng et al., 2006; Jokihaara et al., 2006). Both surgical procedures were conducted at the animal supplier facility one week prior to the arrival of the animals at the laboratory. Animals were weighed each week to assess changes in body mass over the study period. CON, NFR and OVX animals were euthanized via CO_2 inhalation after 2, 3, and 4 months, respectively (based on previous studies assessing the onset of quantifiable manifestations of ovariectomy and partial nephrectomy by our group), and femurs from each animal were used for the study.

2.2. Specimen preparation

After dissection and cleaning of all adherent soft tissues [Fig. 1a – Frame I], the femur was held in a specially designed holding jig. All specimens were cut perpendicular to the anatomic axis using a small diamond wafering blade on a low-speed saw (Isomet, Buehler Corporation, Lake Bluff, IL, USA) under copious irrigation. The first cut was made right above the growth plate proximal to the femoral condyles to include metaphyseal trabecular microstructure [Fig. 1a – Frame II]. The exact location of the first cut was confirmed with anterior–posterior contact radiograph. Then, one thin section less than 1 mm in thickness was cut proximally from the metaphysis and was saved for nano-indentation [Fig. 1a – Frame III]. The femur was then removed from the holding jig and the remaining metaphyseal cortex was shaved off under magnified viewing and ample lighting with the operator holding the femur in hand (allowing much greater freedom of movement than using a jig) [Fig. 1a – Frame IV and V, Appendix for further details]. After removal of the cortex, the femur was placed back in the holding jig and the shaved off metaphyseal (trabecular only) region [H_{TRAB}: 6.22 ± 0.73 mm, $\emptyset_{TRAB}$ at mid-length: 4.84 ± 0.41 mm] was cut [Fig. 1a – Frame VI and Fig. 1b]. Then, a mid-diaphyseal (cortical only) section [H_{CORT}: 5.99 ± 0.28 mm, $\emptyset_{CORT}$ at mid-length: 3.64 ± 0.24 mm] was cut, maintaining an approximate 2:1 height to diameter ratio (Keaveny et al., 1993) [Fig. 1a – Frame VII]. Finally, a thin section less than 1 mm thick was cut from the proximal diaphyseal section for nano-indentation [Fig. 1a – Frame VIII].

The cortical and cancellous specimens underwent cleaning via sonic agitation (Fisher Scientific International, Hampton, NH, USA) while suspended in distilled water for 20 min, followed by centrifugal removal of excess water and marrow at 9G for 15 min. The average mass (m, g) and physical dimensions of each specimen were measured (×3) using precision balance and calipers. Additionally, bone tissue volume (V_{BONE}, mm³) was measured using gas pycnometry (Accupyc 1330, Micromeritics, Norcross, GA, USA).

2.3. Imaging and image analysis

Sequential transaxial images through the entire cortical and cancellous bone sections were obtained using micro-computed tomography (μCT) (μCT 40, Scanco Medical, AG, Brüttisellen, Switzerland) at an isotropic voxel size of 30 μm, integration time of 250 ms and tube voltage and current of 55 KeV and 145 uA, respectively, while applying a 1200 mg cm^{-3} hydroxyapatite (HA) beam hard-ening correction curve. After applying adaptive thresholding [Appendix for further details], cortical (Ct.BV/TV) and trabecular (BV/TV) bone volume fractions were assessed for all images (Hildebrand et al., 1999). Cortical and cancellous equivalent bone mineral densities (ρ_{EQUIV}, g cm^{-3}) were calculated using a hydroxyapatite phantom, supplied by the manufacturer, to convert X-ray attenuation coefficient (μ) to an equivalent density. The variability of μCT assessment of 3D microstructural and densitometric indices of excised rat bone samples is less than 0.5% at our laboratory. The area for each cross-section was calculated by counting the number of voxels and multiplication by pixel size. Then, the cross-section with the minimum area was used to calculate axial stresses. The average
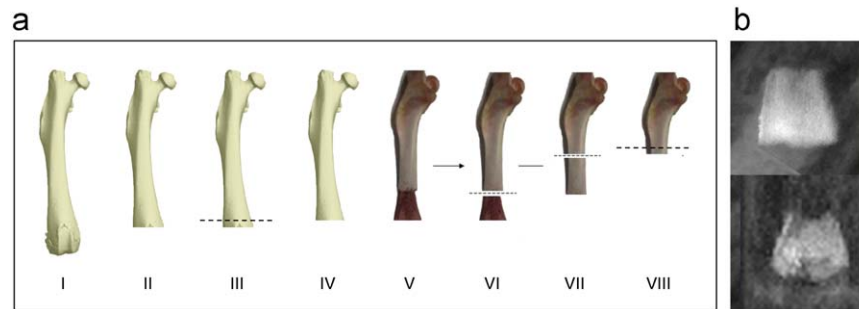
Fig. 1. (a) An illustration of cortical and trabecular specimen preparations for conventional mechanical testing and nano-indentation through a series of frames: (I) whole bone; (II) cut at condyles; (III) distal metaphyseal cut for trabecular nano-indentation; (IV) specimen ready for cortex shaving; (V) distal metaphyseal cortex shaved; (VI) trabecular bone specimen cut; (VII) cortical bone specimen cut; (VIII) two diaphyseal cuts for cortical nano-indentation. (b) Representative distal metaphyseal cancellous bone samples with the cortex shaves from control (left) and ovariectomized (right) animals.
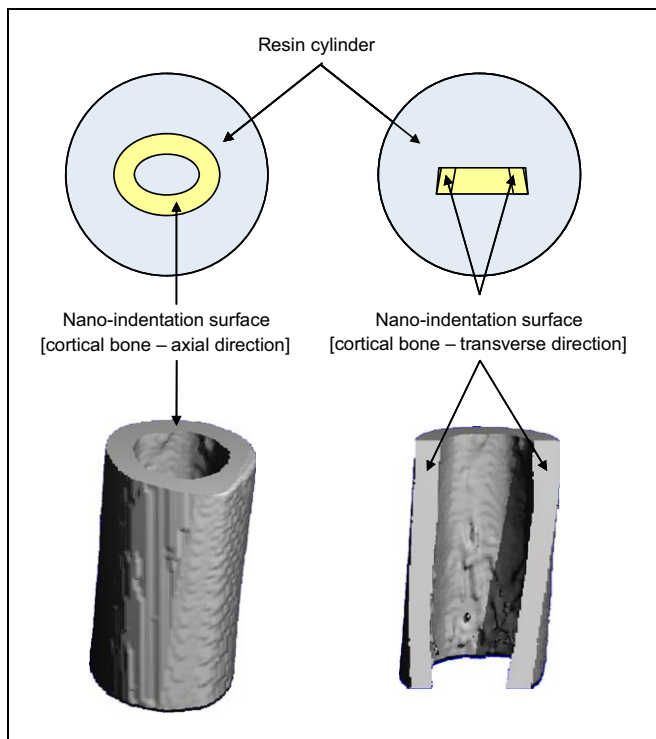

Fig. 2. A depiction of axial and transverse cortical bone samples embedded bone in resin for nano-indentation.

cross-sectional area variation of cortical and trabecular specimens were 6% and 19%, respectively.

2.4. Nano-indentation

The resin embedded cortical and cancellous bone specimens [Fig. 2] were used to assess bone tissue material properties by nano-indentation using a Berkovich indenter (Hysitron Triboindenter System, Minneapolis, Minnesota, USA). The middle of the trabecular elements and the cortical shells were selected as indentation sites to avoid boundary condition errors. Thirty five indentations distributed across the cross-section of each sample were performed and the results were averaged per sample [see Appendix for further details].

2.5. Mechanical testing

Specimens were thawed out to room temperature and hydrated prior to mechanical testing; otherwise, they were stored in saline soaked gauze at -20 °C for the duration of the study. Circular brass end-caps (8 mm in diameter, 1 mm in thickness) were glued to both ends of each sample to reduce end-effect artifacts (Keaveny et al., 1993). Specimens were preconditioned, using a triangular

waveform to 0.33% strain for 7 cycles and a strain rate of 0.005 s^{-1}, followed by uniaxial compression to failure at a strain rate of 0.01 s^{-1} (Instron 8511, Instron, Norwood, MA, USA). Stiffness (K, kN mm^{-1}), yield displacement (d_Y, mm), yield load (L_Y, kN), ultimate displacement (d_{ULT}, mm), ultimate load (L_{ULT}, kN), representing intrinsic structural properties, were reported for the study [Appendix for further details].

2.6. Statistical analysis

Continuous data were assessed for normality using the Kolmogorov–Smirnov test. Bone tissue density (ρ_{TISSUE}, g cm^{-3}) was calculated by dividing bone mass (m) by bone volume (V_{BONE}) obtained through pycnometry, and apparent bone density (ρ_{APP}, g cm^{-3}) was calculated by multiplying bone tissue density (ρ_{TISSUE}) with bone volume fraction (BV/TV or Ct.BV/TV). To assess whether the SD rat bone tissue mechanical properties were different between cortical and cancellous bones, and whether they were affected by orientation, a two-way Analysis of Variance (ANOVA) was conducted with group (cortical or cancellous) and orientation (axial or transverse) as fixed factors and bone tissue properties (tissue modulus and tissue hardness) measured by nano-indentation as dependent parameters.

Univariate regression analysis was conducted to examine whether the modulus of elasticity and yield strength of cortical and cancellous SD rat bone could be expressed as a function of bone volume fraction (obtained from μCT imaging), apparent density, or equivalent bone mineral density (obtained from μCT imaging).

The SPSS statistical package (version 15.0, Chicago, IL, USA) was used for data analysis. All reported p-values are two-tailed with $p < 0.05$ considered statistically significant.

3. Results

There is little difference between normal rat cortical and cancellous tissue properties with respect to tissue type and orientation. Two-way ANOVA results showed that there were no significant differences between the tissue modulus and tissue hardnes values for rat cortical and cancellous bone ($p > 0.05$) and for the orientation ($p > 0.05$). In addition, a paired Student's t test showed no differences in E_{NANO} and H between the pairs of axial ($p = 0.46$) and transverse ($p = 0.72$) specimens for both cortical and cancellous bone [Table 1].

Inclusion of bones from normal, ovariectomized and partially nephrectomized animals resulted in a diverse data set with a bone volume fraction range from 10% to 77% and a bone tissue density range 1.36–2.44 g cm^{-3} [Table 2]. A univariate power law regression model revealed that compressive modulus of elasticity can be expressed as a function of the $\sum \rho_m$ (i) over all pixels (equivalent mineral density) along the cross-section in the form of $E = 8362.8(\rho_{EQUIV})^{2.56}$, $R^2 = 0.77$ [Fig. 3a]. Similarly, compressive yield strength can be expressed as a function of equivalent mineral density in the form of $\sigma_Y = 106.4(\rho_{EQUIV})^{2.21}$, $R^2 = 0.70$ [Fig. 3b]. Moreover, a univariate regression model revealed that compressive modulus of elasticity can be defined

as a function of bone volume fraction in the form of $E = 14899$ $(BV/TV)^{1.94}$, $R^2 = 0.71$ [Fig. 3c]. Similarly, compressive yield strength is defined as a function of bone volume fraction in the form of $\sigma_Y = 180.6(BV/TV)^{1.71}$, $R^2 = 0.68$ [Fig. 3d]. Finally, a univariate regression model revealed that apparent density can describe compressive modulus of elasticity in the form of $E = 3711.4(\rho_{APP})^{1.87}$, $R^2 = 0.74$ [Fig. 3e], and a similar univariate regression model can describe the compressive yield strength of rat bone as a function of apparent density in the form of $\sigma_Y = 53.4(\rho_{APP})^{1.64}$, $R^2 = 0.71$ [Fig. 3f].

4. Discussion

A univariate power law relationship with bone volume fraction, apparent density or equivalent mineral density as the independent variable describes the mechanical properties of rat bone. Either independent variable describes 71–77% of the variation in modulus of elasticity and 68–71% of the variation in yield strength. Each univariate relationship provides a single equation describing the mechanical properties of cortical and cancellous bones precluding the dependence on an arbitrary value to separate cortical from cancellous bone.

The incorporation of pathologic bones from ovariectomized and partially nephrectomized animals enhances the range of bone density and provides a relationship that describes both normal and pathologic bones. In all cases, cancellous bones from OVX animals comprise the lowest density and strength combination, while there is a relative overlap between normal and NFR cancellous bone samples. Additionally, NFR cortical bones encompass the lower density and strength range of the cortical bone distribution; whereas, cortical bones from CON and OVX animals overlap at the higher density strength range of the data distribution. As expected, cancellous bones from OVX animals presented the weakest mechanical properties, as ovariectomy disproportionately affects trabecular microstructure (Wronski et al., 1988; Chen et al., 1995), thereby reducing the load bearing capacity of the cancellous bone. Additionally, partial nephrectomy caused little change in cancellous bone, hence the overlap between cancellous bones from normal and NFR animals (Gal-Moscovici et al., 2002). Moreover, cortical specimens from the NFR group displayed significant decrease in bone volume fraction due to fenestration of the cortical shell in response to the disease [Fig. 4].

The univariate strength equation based on μCT-generated equivalent mineral density provides a convenient means to convert density to strength. This conversion will be useful in studies where the effects of a pathologic condition and/or a pharmacologic agent on the bone strength are examined using the now laboratory standard μCT imaging systems. Likewise, the strength equation based on apparent density provides a conversion means for studies not based on μCT imaging. The strength equation based on bone volume fraction provides a means where strength of bone can be described by the amount of bone present. Such an equation is useful in cases where a pathologic condition or a pharmacologic agent specifically alters the amount of bone.

Table 1
Tissue level mechanical properties of normal (CON) and pathologic (OVX and NFR) rat cortical and cancellous bones in axial and transverse directions (E_{NANO}: tissue modulus, H: tissue hardness).

E_{NANO}(GPa)			H(GPa)
Cortical bone			
Axial	*Mean*	*18.98*	*0.74*
	Standard Deviation	4.78	0.35
Transverse	*Mean*	*17.65*	*0.67*
	Standard Deviation	4.37	0.15
Cancellous bone			
Axial	*Mean*	*18.27*	*0.63*
	Standard Deviation	4.26	0.21
Transverse	*Mean*	*17.08*	*0.62*
	Standard Deviation	4.38	0.19

Table 2
Densitometric and mechanical properties of all cortical and cancellous bones from all three models (CON, OVX and NFR).

	ρ_{TISSUE}(g cm^{-3})	BV/TV (mm^3/mm^3)	ρ_{APP}(g cm^{-3})	ρ_{EQUIV}(gHA cm^{-3})	ε_{YIELD}(%)	σ_{YIELD}(MPa)	ε_{ULT}(%)	σ_{ULT}(MPa)	E(MPa]
Cortical bone									
CON									
Mean	*2.167*	*0.636*	*1.379*	*0.927*	*2.45*	*109.00*	*3.16*	*139.50*	*8803*
Standard Deviation	0.017	0.080	0.174	0.041	0.55	33.82	1.28	19.14	2533
OVX									
Mean	*2.173*	*0.604*	*1.314*	*1.009*	*1.69*	*110.23*	*2.17*	*127.24*	*7256*
Standard Deviation	0.081	0.036	0.101	0.011	0.90	23.94	0.99	35.04	2725
NFR									
Mean	*1.713*	*0.486*	*0.847*	*0.772*	*2.24*	*48.58*	*2.97*	*71.38*	*3442*
Standard Deviation	0.294	0.075	0.248	0.130	1.23	16.26	1.88	33.85	1506
Cancellous bone									
CON									
Mean	*2.156*	*0.366*	*0.788*	*0.563*	*2.01*	*29.95*	*3.90*	*35.95*	*2169*
Standard Deviation	0.072	0.042	0.086	0.073	1.10	12.09	2.82	15.62	916
OVX									
Mean	*2.308*	*0.216*	*0.483*	*0.321*	*2.23*	*18.54*	*3.05*	*26.89*	*1022*
Standard Deviation	0.100	0.077	0.182	0.049	0.82	13.62	1.47	22.35	787
NFR									
Mean	*1.864*	*0.474*	*0.897*	*0.526*	*2.36*	*32.71*	*3.62*	*27.62*	*1912*
Standard Deviation	0.191	0.083	0.217	0.034	1.12	5.74	1.61	10.56	434

The parameters reported in the table are: ρ_{TISSUE}: tissue density, BV/TV: bone volume fraction, ρ_{APP}: apparent density, ρ_{EQUIV}: equivalent density, ε_{YIELD}: yield strain, σ_{YIELD}: yield strength, ε_{ULT}: ultimate strain, σ_{ULT}: ultimate strength, and E: modulus of elasticity.
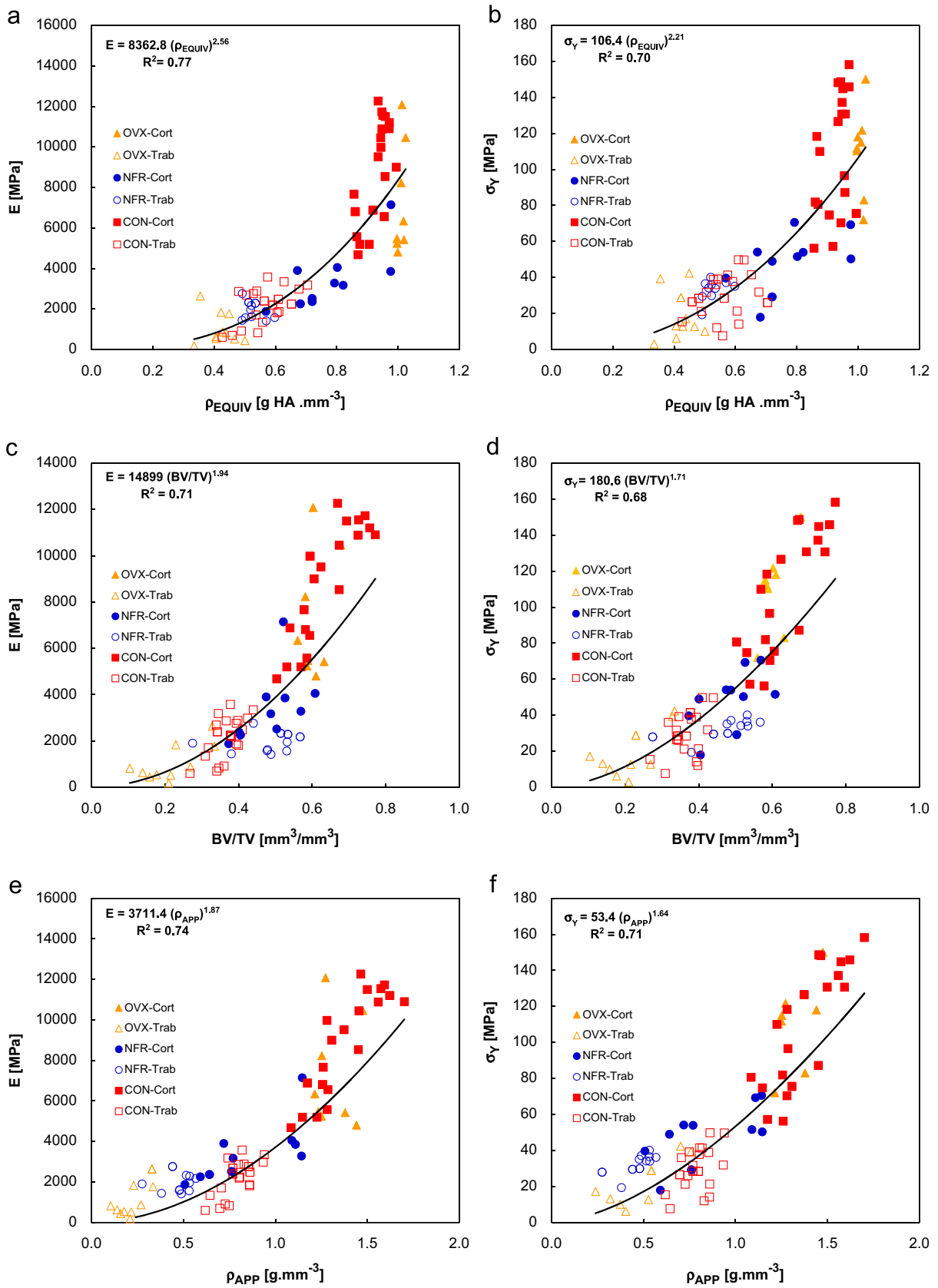
Fig. 3. Univariate exponential relationships describing the mechanical behavior of rat cortical and trabecular bone. (a), (c), and (e) describe modulus of elasticity based on the independent variable of equivalent mineral density, bone volume fraction or apparent density, respectively. Likewise, (b), (d), and (f) describe yield strength based on the independent variable of equivalent mineral density, bone volume fraction or apparent density, respectively.
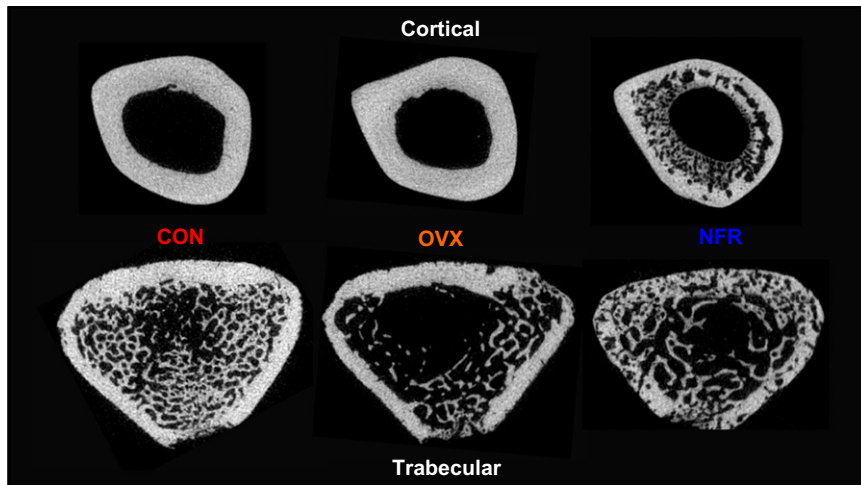
Fig. 4. Representative μCT cross-sections from the mid-diaphysis and from the distal metaphysis illustrate cortical and trabecular bone morphologies, respectively, for CON, OVX and NFR groups. More significant cortical changes are observed in the NFR specimen, yet significant trabecular changes are observed in both the OVX and NFR specimen.

The three relationships presented in this study have been derived from the same animals using the same methods, allowing for cross conversion and interpretation of data, in cases where only one independent variable is available. Further improvement on the predictive powers of these regressions will be achieved by introducing morphometric indices that can better account for the variations in the 3D microstructure of bone (especially cancellous). This step could also reduce the variation in mechanical properties for any given density value.

Mechanical properties of OVX and NFR animal models have been studied previously, but differences in testing modes, specimen preparation protocols, and observation periods makes it difficult to compare those results with the ones generated from this study. Ogoshi et al. (1989) tested metaphyseal and diaphyseal specimens from 24 weeks-old control rat femurs and reported ultimate uniaxial compressive strengths of 126.6 ± 19.7 and 167.3 ± 42.2 MPa, respectively. They tested a distal femur end and a mid-diaphyseal specimen from each femur in compression with constant speed along the specimens' longitudinal axis. The cross sections were imaged and the areas were measured using an ASM Leitz analyzer. We reported σ_{ULT} values of 35.95 ± 15.62 and 139.50 ± 19.14 MPa for cancellous and cortical bones, respectively. There is concordance between the results for diaphyseal cortical bones from the two studies; however, results from metaphyseal bones are significantly higher than those reported for cancellous bones in this study. This discrepancy is due to the fact that metaphyseal bones used in the study by Ogoshi et al. included both cortical cancellous bone components.

Hogan et al. (2000) also studied the mechanical properties of rat cancellous bone. They cut 2 mm long (in axial direction) specimens from the proximal tibia below the growth plate and performed compression testing on the cancellous component of the metaphyseal bone only without disruption of the cortical shell. They reported σ_{ULT} values of 18.1 ± 5.21 MPa for control SD rats. Hogan et al. used the average apparent area to calculate bone strength values which resulted in underestimation of strength and modulus values. In contrast, we have used minimum bone surface area. While minimal cross-sectional area governs the mechanical strength of the structure; calculation of strength should be based on the actual area of bone and not on the apparent area, specially for cancellous bone.

The nano-indentation results suggest that femoral diaphyseal cortical and femoral metaphyseal cancellous SD rat bones have similar tissue level hardness and modulus properties in the axial and transverse directions. Therefore it is reasonable to assume that differences in continuum level modulus properties between the two can be explained by the variations in their respective structures. Additionally, as modulus of elasticity and yield strength are significantly correlated with one another ($R^2=0.92$ in this study), it is assumed that tissue level similarities in modulus will also provide a basis so that continuum level yield strength properties between the two can be explained by the variations in their respective structures. Therefore, it is justified to use a single relationship to describe the mechanical properties of cancellous and cortical bone instead of using an arbitrary value to separate cortical and cancellous bone. This step will help further automate the analysis process, and reduce manual interventions to separate the two types of bones.

The empirical relationships generated in this study to predict bone strength should be interpreted within limitations associated with this type of studies. In order to optimize the utility of an empirical relationship, one should improve the quality of the input sources, which in case of this study are mechanical testing and μCT imaging.

The uniaxial compression was selected as a common mode of mechanical testing for this study which represents a significant portion of in-vivo loads applied to the skeleton (McBroom et al., 1985; Silva et al., 1997). Additionally, it does not require a complex testing setup and can be performed on small specimens. The small specimen size and variations in cross-sectional area could be sources of errors in the mechanical testing..The other source of error in this study is in imaging and analysis methods.

Although there are some limitations in quantitative measurement of bone density with any imaging modality, the current generation of μCT imaging systems' errors in measured density and microstructural data are in the order of 0.5% based on quality control measurements performed in our laboratory (Nazarian et al., 2008).

The univariate relationships based on μCT (ionizing source) generated data can only assess the contribution of the mineral component of the bone to its overall strength, while ignoring the contribution of the matrix. Recent advances in solid state magnetic resonance (MR) imaging have enabled the quantitative assessment of mineral and matrix components of bone using a non-ionizing imaging modality. As the resolution gap between these two modalities is narrowing, it is becoming increasingly possible to establish relationships that account for changes in both mineral and matrix components of bone non-invasively in near future.

There are a number of approaches in virtual biomechanics to determine bone strength from imaging parameters (Lang et al., 1988; Faulkner et al., 1991; Lang et al., 1997; Lang et al., 1998; Beck et al., 2000; Cummings et al., 2002; Riggs and Melton, 2002; Beck, 2003; Heaney, 2003; Bauer et al., 2004; Schuit et al., 2004). One of these approaches is the use of structural rigidity analysis, which is predicated upon the use of empirical relationships to calculate rigidity of each cross-sectional image from the modulus-weighted area of each pixel. The relationships generated from this study can be used to assess rigidity of rat bones as affected by different biologic or pharmaceutical agents. Other approaches are based on the creation of patient specific models from 3D images such as QCT and MRI to predict bone mechanical behavior via finite element (FE) analysis. The correlations reported in this study can be employed in FE models to assign tissue properties to the models and incorporate the effects of density into the existing structure based FE models. In conclusion, we have introduced univariate relationships to describe the mechanical properties of rat bone based on equivalent mineral density, bone volume fraction or apparent density [Fig. 3]. These relationships can describe the mechanical properties of both cortical and cancellous bone over a wide range of bone density and common skeletal pathologies. It is worthwhile to mention that virtual biomechanics is not aimed to replace conventional mechanical testing, as many mechanical properties simply cannot be quantified via virtual biomechanics, such as displacement and absorbed energy. However, virtual biomechanics can provide a first hand and simplified approach to assess the effects of pathology and/or pharmacologic agents on bone strength on a large throughput and cost-effective manner.

Conflict of Interest

None to report.

Acknowledgements

Appendix A. Supplementary material

Supplementary data associated with this article can be found in the online version at doi:10.1016/j.jbiomech.2009.10.047.

References

Aaron, M., Snyder, B.D., Wilson, S., Kwak, D., Zurakowski, D., Coughlin, L, Parker, L, 2002. Noninvasive prediction of fracture risk in patients with metastatic breast cancer to the spine. 47th Annual Meeting of the Orthopedic Research Society, Dallas, TX.

An, Y.H., Friedman, R.J., 1999. In: Animal Models in Orthopaedic Research. CRC Press, Boca Raton.

Ashman, R.B., Rho, J.Y., 1988. Elastic modulus of trabecular bone material. J. Biomech. 21, 177–181.

Bagi, C.M., Miller, S.C., Bowman, B.M., Blomstrom, G.L., France, E.P., 1992. Differences in cortical bone in overloaded and underloaded femurs from ovariectomized rats: comparison of bone morphometry with torsional testing. Bone 13, 35–40.

Bauer, D.C., Black, D.M., Garnero, P., Hochberg, M., Ott, S., Orloff, J., Thompson, D.E., Ewing, S.K., Delmas, P.D., 2004. Change in bone turnover and hip, non-spine, and vertebral fracture in alendronate-treated women: the fracture intervention trial. J. Bone Miner. Res. 19, 1250–1258.

Beck, T., 2003. Measuring the structural strength of bones with dual-energy X-ray absorptiometry: principles, technical limitations, and future possibilities. Osteoporos. Int. 14 (Suppl. 5), 81–88.

Beck, T.J., Looker, A.C., Ruff, C.B., Sievanen, H., Wahner, H.W., 2000. Structural trends in the aging femoral neck and proximal shaft: analysis of the Third National Health and Nutrition Examination Survey dual-energy X-ray absorptiometry data. J. Bone Miner. Res. 15, 2297–2304.

Bessho, M., Ohnishi, I., Matsuyama, J., Matsumoto, T., Imai, K., Nakamura, K., 2007. Prediction of strength and strain of the proximal femur by a CT-based finite element method. J. Biomech. 40, 1745–1753.

Bonnick, S.L., 2007. Noninvasive assessments of bone strength. Curr. Opin. Endocrinol. Diabetes Obes. 14, 451–457.

Borah, B., Gross, G.J., Dufresne, T.E., Smith, T.S., Cockman, M.D., Chmielewski, P.A., Lundy, M.W., Hartke, J.R., Sod, E.W., 2001. Three-dimensional microimaging (MRmicroI and microCT), finite element modeling, and rapid prototyping provide unique insights into bone architecture in osteoporosis. Anat. Rec. 265, 101–110.

Brkovic, D., Linke, J., Jakse, G., Bauss, F., 2005. Changes in bone structure after augmentation cystoplasty in chronic uraemic rats. BJU Int. 95, 1066–1070.

Buckley, J.M., Loo, K., Motherway, J., 2007. Comparison of quantitative computed tomography-based measures in predicting vertebral compressive strength. Bone 40, 767–774.

Chen, M.M., Yeh, J.K., Aloia, J.F., 1995. Effect of ovariectomy on cancellous bone in the hypophysectomized rat. J. Bone Miner. Res. 10, 1334–1342.

Cummings, S.R., Karpf, D.B., Harris, F., Genant, H.K., Ensrud, K., LaCroix, A.Z., Black, D.M., 2002. Improvement in spine bone density and reduction in risk of vertebral fractures during treatment with antiresorptive drugs. Am. J. Med. 112, 281–289.

Danielsen, C.C., Mosekilde, L., Svenstrup, B., 1993. Cortical bone mass, composition, and mechanical properties in female rats in relation to age, long-term ovariectomy, and estrogen substitution. Calcif. Tissue Int. 52, 26–33.

Faulkner, K.G., Glüer, C., Majumdar, S., Lang, P., Engelke, K., Genant, H.K., 1991. Noninvasive measurements of bone mass, structure, and strength: current methods and experimental techniques. Am. J. Radiol. 157, 1229–1237.

Feng, J.Q., Ward, L.M., Liu, S., Lu, Y., Xie, Y., Yuan, B., Yu, X., Rauch, F., Davis, S.I., Zhang, S., Rios, H., Drezner, M.K., Quarles, L.D., Bonewald, L.F., White, K.E., 2006. Loss of DMP1 causes rickets and osteomalacia and identifies a role for osteocytes in mineral metabolism. Nat. Genet. 38, 1310–1315.

Ferretti, J.L., Capozza, R.F., Zanchetta, J.R., 1996. Mechanical validation of a tomographic (pQCT) index for noninvasive estimation of rat femur bending strength. Bone 18, 97–102.

Ferretti, J.L., Gaffuri, O., Capozza, R., Cointry, G., Bozzini, C., Olivera, M., Zanchetta, J.R., Bozzini, C.E., 1995. Dexamethasone effects on mechanical, geometric and densitometric properties of rat femur diaphyses as described by peripheral quantitative computerized tomography and bending tests. Bone 16, 119–124.

Freesmeyer, M.G., Abendroth, K., Faldum, A., Krauss, C., Stein, G., 2001. Comparison of peripheral bone and body axis skeleton in a rat model of mild-to-moderate renal failure in the presence of physiological serum levels of calcitropic hormones. Bone 29, 258–264.

Gal-Moscovici, A., Scherzer, P., Rubinger, D., Weiss, R., Dranitzki-Elhalel, M., Popovtzer, M.M., 2002. Stimulation of osteoclastic bone resorption in a model of glycerol-induced acute renal failure: evidence for a parathyroid hormone-independent mechanism. Bone 31, 488–491.

Gasser, J.A., 1995. Assessing bone quantity by pQCT. Bone 17, 145S–154S.

Genant, H.K., Gordon, C., Jiang, Y., Link, T.M., Hans, D., Majumdar, S., Lang, T.F., 2000. Advanced imaging of the macrostructure and microstructure of bone. Horm. Res. 54 (Suppl. 1), 24–30.

Guldberg, R.E., Hollister, S.J., Charras, G.T., 1998. The accuracy of digital image-based finite element models. J. Biomech. Eng. 120, 289–295.

Guo, X.E., Goldstein, S.A., 2000. Vertebral trabecular bone microscopic tissue elastic modulus and hardness do not change in ovariectomized rats. J. Orthop. Res. 18, 333–336.

Heaney, R.P., 2003. Is the paradigm shifting? Bone 33, 457–465.

Hildebrand, T., Laib, A., Muller, R., Dequeker, J., Ruegsegger, P., 1999. Direct three-dimensional morphometric analysis of human cancellous bone: microstructural data from spine, femur, iliac crest, and calcaneus. J. Bone Miner. Res. 14, 1167–1174.

Hogan, H.A., Ruhmann, S.P., Sampson, H.W., 2000. The mechanical properties of cancellous bone in the proximal tibia of ovariectomized rats. J. Bone Miner. Res. 15, 284–292.

Hong, J., Cabe, G.D., Tedrow, J.R., Hipp, J.A., Snyder, B.D., 2004. Failure of trabecular bone with simulated lytic defects can be predicted non-invasively by structural analysis. J. Orthop. Res. 22, 479–486.

Hornby, S.B., Evans, G.P., Hornby, S.L., Pataki, A., Glatt, M., Green, J.R., 2003. Long-term zoledronic acid treatment increases bone structure and mechanical strength of long bones of ovariectomized adult rats. Calcif. Tissue Int. 72, 519–527.

Ito, M., Nishida, A., Aoyagi, K., Uetani, M., Hayashi, K., Kawase, M., 2005. Effects of risedronate on trabecular microstructure and biomechanical properties in ovariectomized rat tibia. Osteoporos. Int. 16, 1042–1048.

Jamsa, T., Jalovaara, P., Peng, Z., Vaananen, H.K., Tuukkanen, J., 1998. Comparison of three-point bending test and peripheral quantitative computed tomography analysis in the evaluation of the strength of mouse femur and tibia. Bone 23, 155–161.

Jokihaara, J., Jarvinen, T.L., Jolma, P., Koobi, P., Kalliovalkama, J., Tuukkanen, J., Saha, H., Sievanen, H., Kannus, P., Porsti, I., 2006. Renal insufficiency-induced bone

loss is associated with an increase in bone size and preservation of strength in rat proximal femur. Bone 39, 353–360.

Kaczmarczyk-Sedlak, I., Janiec, W., Pytlik, M., Sliwinski, L., Folwarczna, J., Cegeila, U., Nowinska, B., Barnas, M., 2005. Effect of administration of etidronate and retinol on bone mechanical properties in ovariectomized rats. Pharamcol. Rep. 57, 203–211.

Kanis, J.A., Johnell, O., Oden, A., Jonsson, B., De Laet, C., Dawson, A., 2000. Prediction of fracture from low bone mineral density measurements overestimates risk. Bone 26, 387–391.

Kazama, J.J., Iwasaki, Y., Yamato, H., Murayama, H., Sato, M., Gejyo, F., Kurokawa, M., Fukagawa, K., 2003. Microfocus computed tomography analysis of early changes in bone microstructure in rats with chronic renal failure. Nephron Exp. Nephrol. 95, e152–e157.

Keaveny, T.M., Borchers, R.E., Gibson, L.J., Hayes, W.C., 1993. Theoretical analysis of the experimental artifact in trabecular bone compressive modulus. J. Biomech. 26, 599–607.

Keaveny, T.M., Pinilla, T.P., Crawford, R.P., Kopperdahl, D.L., Lou, A., 1997. Systematic and random errors in compression testing of trabecular bone. J. Orthop. Res. 15, 101–110.

Lang, S., Moyle, D., Berg, E., Detorie, N., Gilpin, A., Pappas, N., Reynolds, J., Tkacik, M., Waldron, R., 1988. Correlation of mechanical properties of vertebral trabecular bone with equivalent mineral density as measured by computed tomography. J. Bone Jt. Surg. 70-A, 1531–1538.

Lang, T., Augat, P., Majumdar, S., Ouyang, X., Genant, H.K., 1998. Noninvasive assessment of bone density and structure using computed tomography and magnetic resonance. Bone 22, 149S–153S.

Lang, T.F., Keyak, J.H., Heitz, M.W., Augat, P., Lu, Y., Mathur, A., Genant, H.K., 1997. Volumetric quantitative computed tomography of the proximal femur: precision and relation to bone strength. Bone 21, 101–108.

Leichter, I., Margulies, J.Y., Weinreb, A., Mizrahi, J., Robin, G.C., Conforty, B., Makin, M., Bloch, B., 1982. The relation between bone density, mineral content, and mechanical strength in the femoral neck. Clin. Orthop. Relat. Res. 163, 272–281.

Lochmuller, E.M., Groll, O., Kuhn, V., Eckstein, F., 2002. Mechanical strength of the proximal femur as predicted from geometric and densitometric bone properties at the lower limb versus the distal radius. Bone 30, 207–216.

MacNeil, J.A., Boyd, S.K., 2007. Accuracy of high-resolution peripheral quantitative computed tomography for measurement of bone quality. Med. Eng. Phys. 29, 1096–1105.

Martin, D.E., Severns, A.E., Kabo, J.M., 2004. Determination of mechanical stiffness of bone by pQCT measurements: correlation with non-destructive mechanical four-point bending test data. J. Biomech. 37, 1289–1293.

Martin, R.B., 1991. Determinants of the mechanical properties of bones. J. Biomech. 24 (Suppl. 1), 79–88.

McBroom, R.J., Hayes, W.C., Edwards, W.T., Goldberg, R.P., White 3rd, A.A., 1985. Prediction of vertebral body compressive strength using quantitative computed tomography. J. Bone Jt. Surg. Am. 67, 1206–1214.

Miller, M.A., Chin, J., Miller, S.C., Fox, J., 1998. Disparate effects of mild, moderate, and severe secondary hyperparathyroidism on cancellous and cortical bone in rats with chronic renal insufficiency. Bone 23, 257–266.

Miller, S.C., Wronski, T.J., 1993. Long-term osteopenic changes in cancellous bone structure in ovariectomized rats. Anat. Rec. 236, 433–441.

Moore, G.E., 1965. Cramming more components onto integrated circuits. Electronics 38.

Nazarian, A., Snyder, B.D., Zurakowski, D., Muller, R., 2008. Quantitative micro-computed tomography: a non-invasive method to assess equivalent bone mineral density. Bone 43, 302–311.

Newitt, D.C., van Rietbergen, B., Majumdar, S., 2002. Processing and analysis of in vivo high-resolution MR images of trabecular bone for longitudinal studies: reproducibility of structural measures and micro-finite element analysis derived mechanical properties. Osteoporos. Int. 13, 278–287.

Odgaard, A., Linde, F., 1991. The underestimation of Young's modulus in compressive testing of cancellous bone specimens. J. Biomech. 24, 691–698.

Ogawa, K., Hori, M., Takao, R., Sakurada, T., 2005. Effects of combined elcatonin and alendronate treatment on the architecture and strength of bone in ovariectomized rats. J. Bone Miner. Metab. 23, 351–358.

Ogoshi, K., Moriyama, T., Nanzai, Y., 1989. Decrease in the mechanical strength of bones of rats administered cadmium. Arch. Toxicol. 63, 320–324.

Reddy Nagareddy, P., Lakshmana, M., 2005. Assessment of experimental osteoporosis using CT-scanning, quantitative X-ray analysis and impact test in calcium deficient ovariectomized rats. J. Pharmacol. Toxicol. Methods 52, 350–355.

Rho, J.-Y., Tsui, T.Y., Pharr, G.M., 1998. Elastic properties of human cortical and trabecular lamellar bone measured by nanoindentation. Biomaterials 18, 1325–1330.

Rice, J.C., Cowin, S.C., Bowman, J.A., 1988. On the dependence of the elasticity and strength of cancellous bone on apparent density. J. Biomech. 21, 155–168.

Riggs, B.L., Melton 3rd, L.J., 2002. Bone turnover matters: the raloxifene treatment paradox of dramatic decreases in vertebral fractures without commensurate increases in bone density. J. Bone Miner. Res. 17, 11–14.

Ruegsegger, P., Koller, B., Müller, R., 1996. A microtomographic system for the nondestructive evaluation of bone architecture. Calcif. Tissue Int. 58, 24–29.

Schuit, S.C., van der Klift, M., Weel, A.E., de Laet, C.E., Burger, H., Seeman, E., Hofman, A., Uitterlinden, A.G., van Leeuwen, J.P., Pols, H.A., 2004. Fracture incidence and association with bone mineral density in elderly men and women: the Rotterdam Study. Bone 34, 195–202.

Silva, M., Keaveny, T., Hayes, W., 1997. Load sharing between the shell and centrum in the lumbar vertebral body. Spine 22, 140–150.

Snyder, B.D., Hauser-Kara, D.A., Hipp, J.A., Zurakowski, D., Hecht, A.C., Gebhardt, M.C., 2006. Predicting fracture through benign skeletal lesions with quanti-tative computed tomography. J. Bone Jt. Surg. Am. 88, 55–70.

Snyder, S.M., Schneider, E., 1991. Estimation of mechanical properties of cortical bone by computed tomography. J. Orthop. Res. 9, 422–431.

Turner, C., 1989. Yield behavior of bovine cancellous bone. J. Biomech. Eng. 111, 256–260.

Turner, C.H., 2002. Determinants of skeletal fragility and bone quality. J. Musculoskeletal Neuronal Interact. 2, 527–528.

Turner, C.H., Burr, D.B., 1993. Basic biomechanical measurements of bone: a tutorial. Bone 14, 595–608.

Turner, C.H., Owan, I., Brizendine, E.J., Zhang, W., Wilson, M.E., Dunipace, A.J., 1996. High fluoride intakes cause osteomalacia and diminished bone strength in rats with renal deficiency. Bone 19, 595–601.

Turner, C.H., Rho, J., Takano, Y., Tsui, T.Y., Pharr, G.M., 1999. The elastic properties of trabecular and cortical bone tissues are similar: results from two microscopic measurement techniques. J. Biomech. 32, 437–441.

Un, K., Bevill, G., Keaveny, T.M., 2006. The effects of side-artifacts on the elastic modulus of trabecular bone. J. Biomech. 39, 1955–1963.

van Rietbergen, B., Majumdar, S., Newitt, D., MacDonald, B., 2002. High-resolution MRI and micro-FE for the evaluation of changes in bone mechanical properties during longitudinal clinical trials: application to calcaneal bone in postmeno-pausal women after one year of idoxifene treatment. Clin. Biomech. (Bristol., Avon.) 17, 81–88.

Van Rietbergen, B., Muller, R., Ulrich, D., Ruegsegger, P., Huiskes, R., 1999. Tissue stresses and strain in trabeculae of a canine proximal femur can be quantified from computer reconstructions. J. Biomech. 32, 165–173.

Wang, L., Orhii, P.B., Banu, J., Kalu, D.N., 2001. Effects of separate and combined therapy with growth hormone and parathyroid hormone on lumbar vertebral bone in aged ovariectomized osteopenic rats. Bone 28, 202–207.

Whealan, K.M., Kwak, S.D., Tedrow, J.R., Inoue, K., Snyder, B.D., 2000. Noninvasive imaging predicts failure load of the spine with simulated osteolytic defects. J. Bone Jt. Surg. Am. 82, 1240–1251.

Wronski, T.J., Cintron, M., Dann, L.M., 1988. Temporal relationship between bone loss and increased bone turnover in ovariectomized rats. Calcif. Tissue Int. 43, 179–183.

Yao, W., Hadi, T., Jiang, Y., Lotz, J., Wronski, T.J., Lane, N.E., 2005. Basic fibroblast growth factor improves trabecular bone connectivity and bone strength in the lumbar vertebral body of osteopenic rats. Osteoporos. Int. 16, 1939–1947.

Zysset, P.K., Guo, X.E., Hoffler, C.E., Moore, K.E., Goldstein, S.A., 1999. Elastic modulus and hardness of cortical and trabecular bone lamellae measured by nanoindentation in the human femur. J. Biomech. 32, 1005–1012.